Am J Physiol Renal Physiol 318: F1284–F1294, 2020.
First published March 23, 2020; doi:10.1152/ajprenal.00030.2020.

RESEARCH ARTICLE

Distinct functions of megalin and cubilin receptors in recovery of normal and nephrotic levels of filtered albumin

Qidong Ren,[1,2] Kathrin Weyer,[3] Youssef Rbaibi,[2] Kimberly R. Long,[2] Roderick J. Tan,[2] Rikke Nielsen,[3] Erik I. Christensen,[3] Catherine J. Baty,[2] Ossama B. Kashlan,[2] and Ora A. Weisz[2]

[1]*School of Medicine, Tsinghua University, Beijing, China;* [2]*Renal-Electrolyte Division, Department of Medicine, University of Pittsburgh School of Medicine, Pittsburgh, Pennsylvania; and* [3]*Department of Biomedicine, Aarhus University, Aarhus, Denmark*

Submitted 21 January 2020; accepted in final form 10 March 2020

Ren Q, Weyer K, Rbaibi Y, Long KR, Tan RJ, Nielsen R, Christensen EI, Baty CJ, Kashlan OB, Weisz OA. Distinct functions of megalin and cubilin receptors in recovery of normal and nephrotic levels of filtered albumin. *Am J Physiol Renal Physiol* 318: F1284–F1294, 2020. First published March 23, 2020; doi:10.1152/ajprenal.00030.2020.—Proximal tubule (PT) cells express a single saturable albumin-binding site whose affinity matches the estimated tubular concentration of albumin; however, albumin uptake capacity is greatly increased under nephrotic conditions. Deciphering the individual contributions of megalin and cubilin to the uptake of normal and nephrotic levels of albumin is impossible in vivo, as knockout of megalin in mice globally disrupts PT endocytic uptake. We quantified concentration-dependent albumin uptake in an optimized opossum kidney cell culture model and fit the kinetic profiles to identify albumin-binding affinities and uptake capacities. Mathematical deconvolution fit best to a three-component model that included saturable high- and low-affinity uptake sites for albumin and underlying nonsaturable uptake consistent with passive uptake of albumin in the fluid phase. Knockdown of cubilin or its chaperone amnionless selectively reduced the binding capacity of the high-affinity site, whereas knockdown of megalin impacted the low-affinity site. Knockdown of disabled-2 decreased the capacities of both binding sites. Additionally, knockdown of megalin or disabled-2 profoundly inhibited the uptake of a fluid phase marker, with cubilin knockdown having a more modest effect. We propose a novel model for albumin retrieval along the PT in which cubilin and megalin receptors have different functions in recovering filtered albumin in proximal tubule cells. Cubilin binding to albumin is tuned to capture normally filtered levels of the protein. In contrast, megalin binding to albumin is of lower affinity, and its expression is also essential for enabling the recovery of high concentrations of albumin in the fluid phase.

amnionless; cubilin; disabled-2; endocytosis; megalin; proteinuria; proximal tubule

INTRODUCTION

The proximal tubule (PT) of the kidney maintains stable fractional solute and fluid reabsorption over a wide range of glomerular filtration rates to preserve glomerulotubular balance. In addition to reabsorbing the majority of filtered water, Na^+, glucose, and other solutes, cells that comprise the S1 and S2 segments of the proximal convoluted tubule internalize essentially all proteins that escape the glomerular filtration barrier to maintain a nearly protein-free urine. The large multiligand receptors megalin [low-density lipoprotein-related protein 2 (*LRP2*)] and cubilin (*CUBN*), expressed at the apical surface of these cells, bind to and internalize >50 different plasma proteins (7, 15). Megalin is a ~600-kDa type 1 transmembrane protein related to the low-density lipoprotein receptor. The cytoplasmic domain of megalin contains two NPXY motifs that engage the clathrin adaptor disabled-2 (Dab2) and mediate endocytosis of the protein into apical endocytic compartments. Cubilin (~460 kDa) lacks a transmembrane domain and requires association with amnionless (AMN; ~50 kDa) to reach the apical membrane as a CUBAM complex (9, 10, 46). Like megalin, AMN also contains Dab2-binding motifs that are able to mediate CUBAM internalization in cells and tissues that do not express megalin (12, 22, 38, 39). Loss of either megalin or cubilin expression results in tubular proteinuria (27, 36), and biochemical and morphological studies have suggested that they function as a complex in the PT (1, 30). However, whether direct interaction with megalin is required for cubilin function in the PT is not known.

Plasma albumin levels in adult rats are ~2.6 g/dL (433 μM) (51), and the majority of micropuncture and other studies in the rat have suggested that the slit diaphragm provides an effective barrier to albumin, with only ~23 μg/mL (0.4 μM) albumin present in the filtrate (47). Consistent with this, albumin binds to the apical surface of opossum kidney (OK) PT cells via a saturable high-affinity site (half-maximal binding ~20–30 μg/mL or 0.3–0.45 μM) (17, 44) that seems ideally tuned to capture normally filtered levels of this ligand. The apparent match between tubular levels of albumin and the binding affinity for receptors on the apical surface of PT cells makes physiological sense but raises an underappreciated conundrum: if albumin binding is saturated at this low (normal) concentration, then why are elevated levels of albumin cytotoxic to the PT? Recent experiments have confirmed large increases in albumin accumulation in the PTs of rodents when the glomerular filtration barrier is compromised (35, 48, 49). While knockout (KO) of megalin and cubilin increased urinary albumin levels by ~20-fold, disruption of the glomerular filtration barrier by KO of podocin resulted in an ~3,000-fold increase in urinary albumin. Remarkably, KO of megalin and cubilin in addition to podocin led to an additional 40% increase in albumin excretion, suggesting that the capacity for PT albumin uptake in nephrotic conditions is vastly beyond that needed to maintain a protein-free urine in the normally functioning kidney. The increased albumin uptake capacity in nephrotic PTs does not require in-

Correspondence: O. A. Weisz (e-mail: weisz@pitt.edu).

creased expression of megalin or cubilin, as mRNA levels of both *LRP2* and *CUBN* were unchanged in podocin KO mice relative to controls (49).

High-capacity albumin uptake has also been demonstrated in isolated perfused rabbit tubules, where increasing uptake of radioiodinated albumin delivered at concentrations up to 2 mg/mL was observed (37). The authors speculated that high-capacity uptake occurred via fluid phase endocytosis. However, fluid phase uptake has generally been considered to have a negligible contribution to the physiological uptake of filtered proteins by PT cells (8, 29, 44).

Understanding the mechanisms and pathways that mediate albumin uptake in the PT is important for designing interventions to treat proteinuric disease. Dissecting the role of megalin and CUBAM receptors in albumin recovery using animal KO models has proven challenging, as KO of megalin or Dab2 in vivo results in a dramatic reduction in PT apical endocytic compartments, with a concomitant increase in urinary protein excretion (27, 33, 34). As an alternative approach, we have modeled concentration-dependent albumin uptake in an optimized cell culture model of the PT. Using siRNA-mediated knockdown, we established the roles of cubilin, megalin, and Dab2 in the uptake of normally filtered and nephrotic levels of albumin. Together with experiments in mouse KO models, the results of our study suggest a new model to explain the remarkable ability of PT cells to recover albumin over the broad range of filtered concentrations in normal and pathological conditions.

MATERIALS AND METHODS

Cell culture and siRNA. OK cells (RRID:CVCL_0472, female) were cultured on Transwell filters under continuous orbital shear stress at 146 rpm as previously described (28). For RNA inhibition experiments, 1 μg siRNA (Dharmacon) and 1.5 μL Lipofectamine RNAiMAX transfection reagent (ThermoFisher) were added separately to Opti-MEM reduced serum medium (ThermoFisher), mixed together (250 μL total) for 15 min, and then added to the apical chamber of a filter support containing freshly plated OK cells {4×10^5 cells/filter in 250 μL growth medium [DMEM-F-12 (D6421, Sigma) supplemented with 5% FBS (S11150, Atlanta Biologicals) and 5 mM glutaMAX (no. 35050-061, GIBCO), pH 7.2–7.5]}. The siRNA sequences used in this study are shown in Supplemental Table S1 in the Supplemental Material (all Supplemental Material is available at https://doi.org/10.6084/m9.figshare.12169476.v1). The medium was changed after 6 h, and cells were transfected again the following day and shifted to culture under orbital shear stress. The medium was changed after 6 h and then daily for an additional 72 h before experiments began. Where indicated, knockdown was confirmed by indirect immunofluorescence and Western blot analysis as previously described using anti-megalin antibody generously provided by Dr. Daniel Biemesderfer, a new anti-cubilin antibody validated in Supplemental Fig. S1, or anti-Dab-2 antibody (no. 12906, Cell Signaling) (28, 52). Relative quantification (comparative C_q method) for quantitative PCR was performed using iTaq Universal SYBR Green Supermix 500 (no. 1725121, Bio-Rad) on a CFX Connect Real-Time PCR Detection System (Bio-Rad) to assess the effect of each siRNA on transcript levels of *CUBN*, *AMN*, and megalin (*LRP2*). Primers were designed by Primer-Blast (National Center for Biotechnology Information) using default settings and validated by agarose gel electrophoresis. The housekeeping gene β-actin (*ACTB*) was used as an internal reference.

Albumin uptake assays. OK cells cultured on filters under orbital shear stress for 72 h as described above were incubated for 15 min at 37°C under continuous orbital shear stress with Alexa Fluor 647-albumin (A34785, Invitrogen) added apically in serum-free growth medium supplemented with 25 mM HEPES (pH 7.2–7.5). Filters were washed three times with cold PBS (with Mg^{2+} and Ca^{2+}), filters were excised with a razor blade, and cells were solubilized in 300 μL MOPS buffer [20 mM MOPS in 0.1% (vol/vol) Triton X-100, pH 7.4] for 30 min on a shaker at 4°C. Cell-associated Alexa Fluor 647 fluorescence intensity was quantified by spectrofluorimetry.

Modeling albumin uptake. Albumin uptake data were modeled using the Hill-Langmuir equation and Igor Pro 6.37 (Wavemetrics, Oswego, OR), using custom functions and the program's built-in global fitting routine. We hypothesized that EC_{50} values (K_1, K_2, etc.) were intrinsic to specific uptake pathways and that attendant maximum velocities (V_1, V_2, etc.) reflected the contribution of each pathway to overall uptake. Cooperativity was also considered and treated as intrinsic to specific pathways, giving the following equation:

$$\sum_{i=1}^{n} \frac{V_i}{1 + \left(\frac{K_i}{\text{albumin concentration}} \right)^{H_i}}$$

Accordingly, K values and Hill coefficients (H_1, H_2, etc.) were common parameters to all experiments (i.e., global parameters), while V values were unique parameters for each experiment (i.e., local parameters). The three-pathway model ($n = 3$) with no Hill coefficients fit the data significantly better than any of the simpler models (see Supplemental Fig. S2).

Immunofluorescence staining in KO mouse models. Generation, breeding, and urinary albumin excretion levels of podocin-, megalin-, and cubilin-inducible KO mice have been previously described (32, 49, 50). Mouse breeding and experiments were carried out in a certified animal facility according to the Danish Animal Experiments Inspectorate. Female tamoxifen-inducible UBC-cre/ERT2 transgenic mice (Jackson Laboratory) were used for experiments at ages of 8–12 wk. Podocin KO ($Nph2^{lox/lox}$;Cre+), cubilin KO ($Cubn^{lox/lox}$;Cre+), megalin KO ($Meg^{lox/lox}$;Cre+), cubilin/podocin KO ($Cubn^{lox/lox}$, $Nph2^{lox,lox}$;Cre+), megalin/podocin KO ($Meg^{lox/lox}$,$Nph2^{lox,lox}$;Cre+), and control mice ($Meg^{lox/lox}$,$Cubn^{lox/lox}$,$Nph2^{lox,lox}$;Cre−), were induced by intraperitoneal injection of tamoxifen (Sigma-Aldrich) at a dose of 33 mg/kg body wt for 5 consecutive days. Knockdown of the target genes in the kidneys was verified by quantitative real-time PCR as previously described (49) and immunohistochemistry at *week 5* of the experiment (counting from the first day of tamoxifen induction). At termination, mice were anesthetized using isoflurane and kidneys were fixed by retrograde perfusion through the abdominal aorta with 2% paraformaldehyde in 0.1 M sodium cacodylate buffer (pH 7.4). Afterward, kidneys were dehydrated, embedded in paraffin, and cut into 2-μm sections using standard methods. For immunofluorescence labeling, kidney paraffin sections were incubated with primary antibodies at 4°C overnight followed by incubation with secondary antibodies for 1 h at ambient temperature as previously described (35). Immunofluorescence images were taken using a confocal laser-scanning microscope (LSM 510-META, Carl Zeiss) and processed using Zeiss Zen software (Light Edition). The primary antibodies used were sheep anti-rat megalin (31), Alexa Fluor 488-conjugated rabbit anti-rat cubilin (42), and rabbit anti-human albumin (A0001, DAKO). The secondary antibodies used were donkey anti-rabbit Alexa Fluor 594 (no. 21207, Invitrogen) and donkey anti-sheep Alexa Fluor 680 (no. 21102, Invitrogen).

Quantitation of megalin-to-cubilin transcript ratios by digital PCR. Droplet digital PCR was performed using cDNA prepared from OK cells and the mouse kidney cortex using a QX100 system (Bio-Rad) according to the manufacturer's specifications. The sequences used are provided in Supplemental Table S3. Mouse droplet digital PCR (ddPCR) primers and probes were designed and verified by Bio-Rad.

Custom probe-based quantitative PCR assays were designed using the Integrated DNA Technologies RealTime qPCR Assay tool with default settings. Consensus sequences for *LRP2* and *CUBN* genes obtained from the de novo transcriptome of a female *Didelphis virginiana* (opossum) PT cell line (14) were entered into the Integrated DNA Technologies tool as single exons because the location of intron/exon junctions are not clearly defined for this model organism. As a result, it is unclear whether assays span an intron-exon junction. Therefore, downstream experiments included aliquots of each sample for which reverse transcription was omitted to control for contaminating DNA in the RNA preparation. *LRP2* and *CUBN* probes were labeled with HEX and 6-FAM fluorophores, respectively, and assays were optimized by ddPCR amplification across a temperature gradient (49.9–62°C) with 1 ng cDNA to determine the optimum annealing temperature for the assays. PCRs contained 1× ddPCR Supermix for Probes (Bio-Rad), 1× primer/probe mix for both assays, and 3 ng cDNA in a 25-μL reaction volume. Twenty microliters were loaded into the droplet generator to create a digital PCR emulsion. PCR was performed on a MasterCyclerPro (Eppendorf). Following 10 min of enzyme activation, PCR conditions were 40 cycles of (94°C 30 s, 58°C 1 min, and 98°C 10 min). After PCR, droplets were loaded on the QX100 Droplet Reader. Analysis with QuantaSoft Analysis Pro 1.0.596 software (Bio-Rad) returned copies per microliter.

Statistics. Unless otherwise noted, data were plotted and statistical significance was assessed using Prism software (GraphPad).

RESULTS

Multiple pathways mediate dose-dependent albumin uptake. We previously observed that OK cells cultured on Transwell supports under continuous orbital shaking develop the uniquely differentiated morphological specializations observed in PT cells in vivo (28, 41). These cells exhibit increased expression of megalin, cubilin, and Dab2 mRNA compared with OK cells maintained under static conditions (unpublished observations) and have an approximately fivefold higher apical endocytic capacity (28). Additionally, cells cultured in this manner develop the robust oxidative metabolism needed to drive PT ion transport and endocytic capacity (41).

Similar to PT cells in vivo, OK cells internalized considerably more apically added albumin when exposed to high concentrations (2 mg/mL) compared with concentrations predicted to be normally filtered by the glomerulus (50 μg/mL; Fig. 1*A*). To quantitate the dose dependence of albumin uptake, we incubated OK cells with increasing concentrations of Alexa Fluor 647-albumin at 37°C for 15 min and then measured cell-associated albumin in cell lysates by spectrofluorimetry. As shown in the representative experiment in Fig. 1*B*, albumin uptake increased rapidly with concentration before leveling off, although uptake continued to increase even at very high concentrations (5 mg/mL). Notably, the kinetic profile did not resemble the classic Michaelis-Menten kinetic profile typical of ligand binding to a single site. We reproducibly observed an inflection in the rate of albumin uptake between 350 and 750 μg/mL albumin, suggesting that at least two pathways of differing affinities contributed to the kinetic profile (see Supplemental Fig. S3). Preliminary fits of the data (the final fit determined as described below is shown in Fig. 1*B*) suggested multiple uptake components with distinct apparent affinities: a high-affinity component (C_1) with a ~50 μg/mL affinity constant, a low-affinity component (C_2) with a ~300 μg/mL affinity constant, and a nonsaturable component (C_3). A semi-log plot of the fit is shown in Fig. 1*C* to better highlight the low-affinity component, which is more difficult to visualize in linear graphs. Control experiments confirmed that C_1 and C_2 components are saturable, as uptake of Alexa Fluor 647-albumin was virtually abolished in the presence of 100 mg/mL unlabeled albumin (see Supplemental Fig. S3). In contrast, uptake via the C_3 component was unaffected by excess unla-

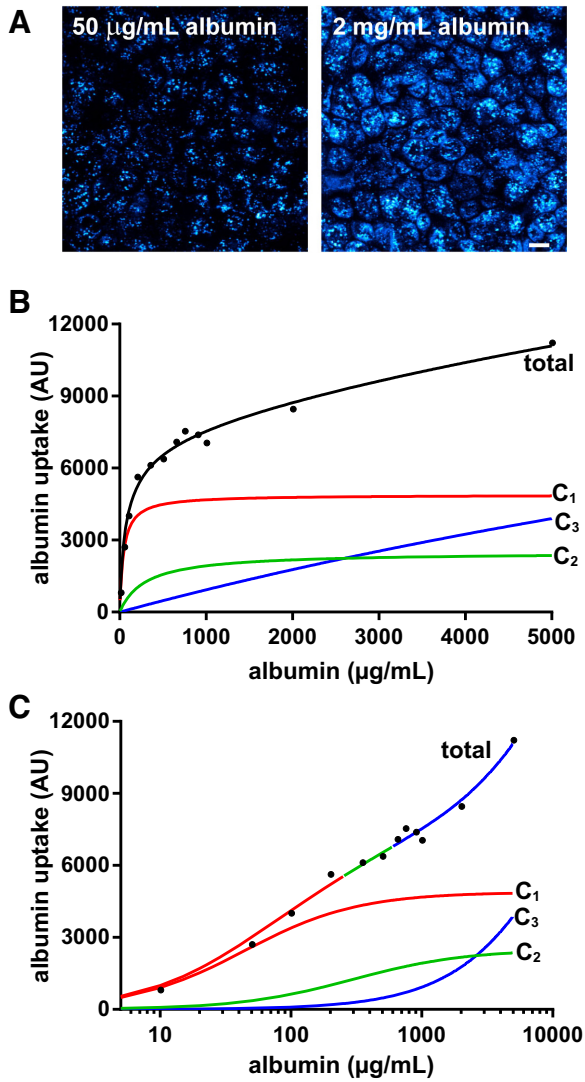

Fig. 1. Three pathways mediate dose-dependent albumin uptake by opossum kidney (OK) cells. *A*: OK cells incubated with 50 μg/mL albumin or 2 mg/mL albumin were fixed and visualized by confocal microscopy. Images were acquired and processed identically, and a maximum projection of a representative field is shown. Scale bar = 10 μm. *B*: OK cells were incubated with the indicated concentrations of Alexa Fluor 647-albumin at 37°C for 15 min and then rapidly washed and solubilized, and cell-associated albumin was assessed by spectrofluorimetry. Global fitting of >30 experiments was used to resolve the curve into three components: saturable high-affinity (C1; red) and low-affinity (C2; green) uptake components and an underlying nonsaturable component (C3; blue) that we attribute to fluid phase uptake. The half-maximal uptake values for the high-affinity and low-affinity components were 44 and 295 μg/mL albumin, respectively, and the respective maximal uptake capacities in this experiment were 4,883 and 2,494. *C*: curves shown in *B* are replotted on a semi-log scale to more easily visualize the three uptake components. The total curve is color coded to show the regions where albumin uptake is dominated by the high-affinity (red), low-affinity (green), or nonsaturable (blue) component. AU, arbitrary units.

beled albumin, as predicted for a fluid phase pathway. We tested the idea of multiple uptake pathways with distinct affinities by knocking down individual components of the uptake machinery as described below.

Knockdown of cubilin, megalin, and Dab2 differentially impair albumin uptake pathways. Albumin and many other filtered ligands bind to both purified cubilin and megalin; however, the role of these individual receptors in uptake is not well understood (5, 11, 27). We developed siRNA oligonucleotides that efficiently depleted expression of cubilin, megalin, or Dab2 and examined the consequences on protein levels by Western blot analysis. As shown in Fig. 2, *A–C* (full-length blots in Supplemental Fig. S4), knockdown of each protein was highly efficient. We also developed a siRNA targeting AMN and confirmed its efficacy using quantitative PCR (see Supplemental Fig. S5*A*). Knockdown of cubilin reduced AMN protein expression and vice versa (Supplemental Figs. S4*A* and S5*B*), consistent with prior reports demonstrating that cubilin and AMN are mutually dependent on one another's expression for efficient maturation and surface delivery (10). In contrast, depletion of megalin or Dab2 did not alter the expression level of the other blotted proteins (Fig. 2, *B* and *C*). Indirect immunofluorescence revealed that knockdown of cubilin, megalin, or Dab2 dramatically reduced the uptake of physiological levels of albumin (Fig. 2, *D–F*). We did notice that the residual albumin staining pattern differed slightly in megalin-deficient cells compared with the other conditions.

Data from >30 experiments quantifying concentration-dependent uptake of albumin in control and siRNA-transfected cells were fit simultaneously to determine the best model that fit the kinetic profile as described in detail in MATERIALS AND METHODS (Supplemental Figs. S2 and S6). The optimal model included saturable high-affinity and low-affinity components with affinity constants K_1 and K_2 of 44 ± 4 and 295 ± 35 μg/mL, respectively, and a nonsaturable pathway (modeled as a curve with K_3 = 20,000 μg/mL) that likely represents fluid phase uptake. The raw data with residuals from all uptake curves are provided in Supplemental Fig. S6, and best-fit curves along with their deconvolved components are shown for control (Fig. 3*A*), cubilin knockdown (Fig. 3*B*), megalin knockdown (Fig. 3*C*), and Dab2 knockdown (Fig. 3*D*) experiments. The high-affinity (C_1) and nonsaturable (C_3) components were readily apparent in the fitted curves, whereas the low-affinity component (C_2) was more easily visualized in semi-log plots of the data (Supplemental Fig. S6). Notably, the C_2 component was more difficult to resolve than the C_1 or C_3 components, as the latter two are isolated at the low and high ends of the uptake curves. This resulted in relatively greater uncertainty in estimating the contribution of the C_2 component. The value we obtained for K_1 was very similar to the single saturable ~50 μg/mL K_m binding site for albumin previously described in OK cells (17), which we confirmed in our cell culture model (K_m = 49 μg/mL; Supplemental Fig. S7), whereas K_2 was apparently too weak to measure using surface binding assays.

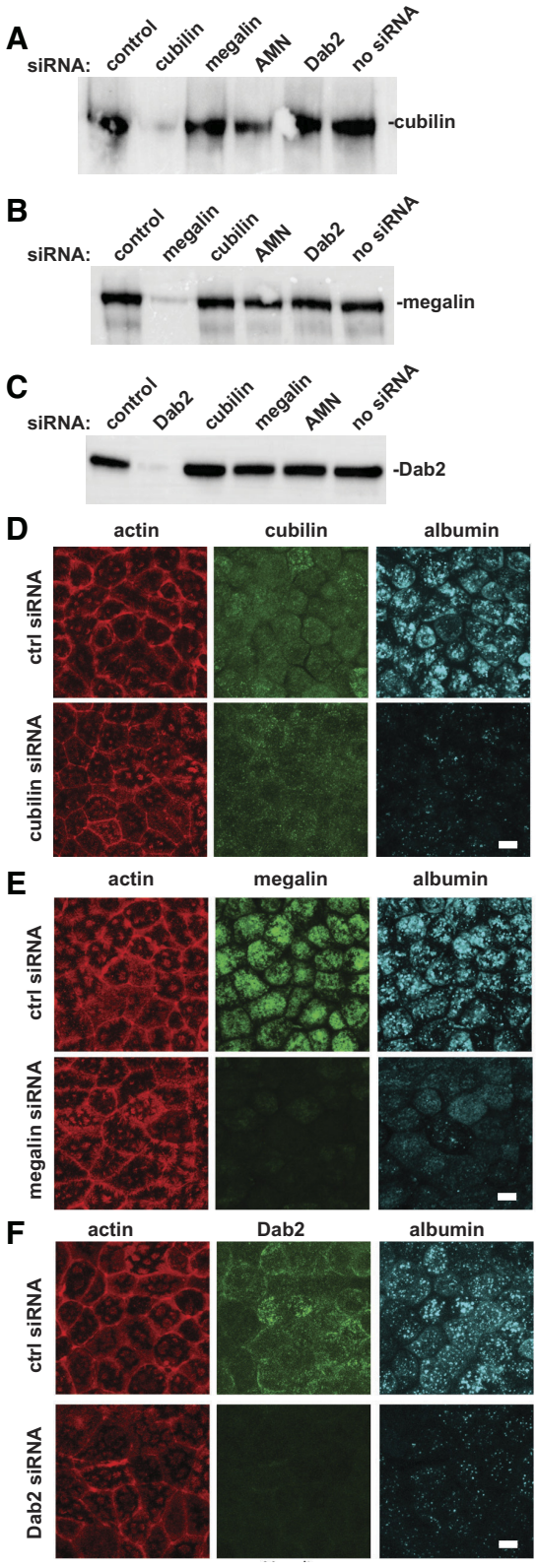

Fig. 2. Efficient knockdown of megalin, cubilin, and disabled-2 (Dab2) impairs uptake of physiological concentrations of filtered albumin. Cells were transfected with the indicated siRNAs and cultured on Transwells as described in MATERIALS AND METHODS. Samples were solubilized, and equal protein loads were run on SDS-PAGE and Western blotted to detect cubilin (*A*), megalin (*B*), or Dab2 (*C*). Similar results were observed in 2 independent experiments. Opossum kidney cells transfected with the indicated siRNAs were incubated with 50 μg/mL Alexa Fluor 647-albumin for 15 min, fixed, and then processed to detect actin and cubilin (*D*), megalin (*E*), or Dab2 (*F*). Scale bar = 10 μm. ctrl, control.

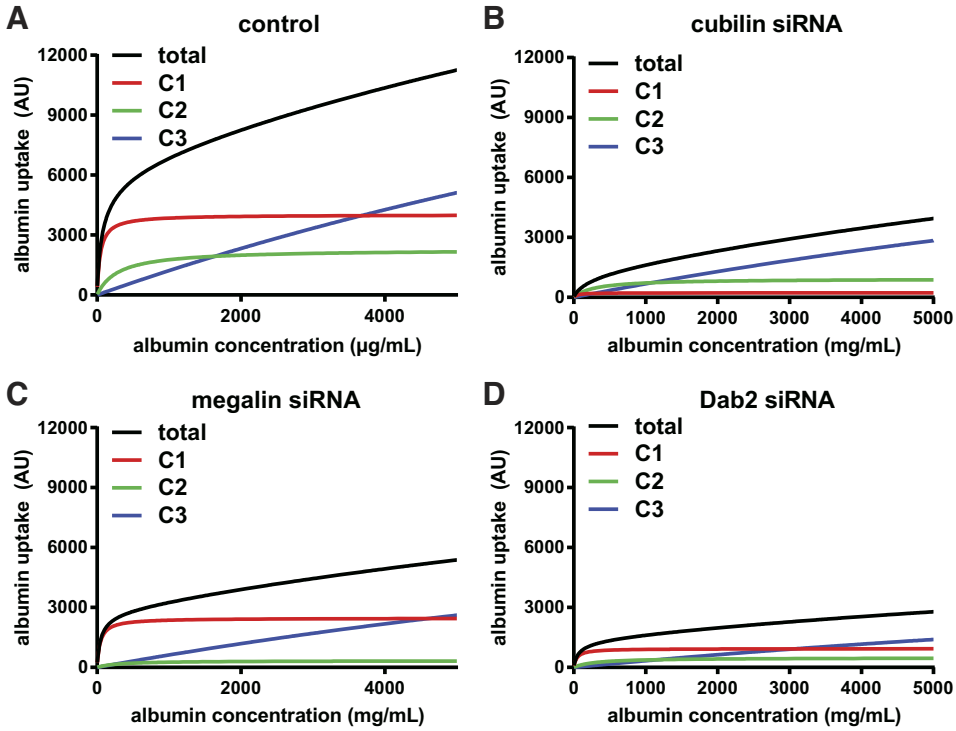

Fig. 3. Knockdown of cubilin, megalin, and disabled-2 (Dab2) differentially affect albumin uptake via high- and low-affinity pathways. The average (black) curves and individual components (C1, red; C2, green; and C3, blue) obtained by fitting the average kinetic profiles of albumin uptake in control (*A*), cubilin siRNA (*B*), megalin siRNA (*C*), and Dab2 siRNA (*D*) data sets are plotted. AU, arbitrary units.

Cubilin knockdown caused a significant reduction in overall uptake (average 39% of control uptake at 5 mg/mL albumin, $n = 8$, $P \leq 0.0005$ by one-way ANOVA with Dunnett's post hoc test; Fig. 3*B*). In particular, we noted a shift to the right at low albumin concentrations, suggesting selective reduction of a high-affinity uptake pathway. At 50 μg/mL, albumin uptake in cubilin knockdown cells was only 11.5% of control uptake ($P \leq 0.0002$). As expected, knockdown of AMN essentially phenocopied the effect of cubilin siRNA on albumin uptake (Supplemental Fig. S5*C*).

In contrast to cells treated with cubilin or AMN siRNA, albumin uptake in cells treated with megalin siRNA rose steeply at low concentrations, suggesting that the high-affinity component was not impacted by megalin knockdown. Albumin uptake at 50 μg/mL in cells treated with megalin siRNA was 55% of control levels ($n = 6$, $P = 0.075$), in contrast to the nearly 90% reduction we measured in cubilin-depleted cells. At high concentrations of albumin (5 mg/mL), uptake in megalin knockdown cells was reduced to 47.0% of control ($P \leq 0.005$).

Dab2 binds to NPXY motifs on the cytoplasmic tails of proteins and links these to the endocytic machinery. Knockdown of Dab2 is thus expected to inhibit endocytic uptake of CUBAM and megalin to a similar extent. Additionally, knockdown of Dab2 has been demonstrated to dramatically reduce the number of clathrin-coated pits and apical endocytic vesicles in the PT (33). Consistent with this, the global fit of data from multiple experiments revealed a dose-dependent curve for albumin uptake that was very similar to that of control cells, albeit with profoundly reduced capacities for all components (Fig. 3*D*).

Figure 4 shows the effect of cubilin, AMN, megalin, and Dab2 knockdown on the maximal uptake capacities of the high-affinity and low-affinity components (V_1 and V_2, respectively). Whereas cubilin or AMN knockdown caused a significant reduction in V_1, megalin knockdown did not significantly affect the capacity of the high-affinity site (Fig. 4*A*). This suggests that CUBAM receptors are capable of internalizing albumin in PT cells independently of megalin. In contrast, megalin knockdown selectively impaired the maximal uptake capacity of the low-affinity component (V_2; Fig. 4*B*). As predicted, Dab2 knockdown reduced both V_1 and V_2, consistent with its effect on both cubilin- and megalin-mediated uptake (Fig. 4, *A* and *B*).

Since knockdown of CUBAM or megalin had selective effects on V_1 and V_2, the relative uptake capacities of each component changed accordingly. The average V_2-to-V_1 ratio (V_2/V_1) in control OK cells was 0.57 and increased upon knockdown of cubilin to 3.9 (Fig. 4*C*). Knockdown of AMN, which should phenocopy the effect of cubilin depletion, resulted in a similar increase in V_2/V_1 to 4.1. In contrast, knockdown of megalin reduced V_2/V_1 to 0.14 (Fig. 4*C*). Consistent with its role in capturing CUBAM and megalin receptors into clathrin-coated pits, the average V_2/V_1 in Dab2 knockdown cells (0.51) was essentially unchanged compared with control cells (Fig. 4*C*).

Cubilin is dispensable for PT accumulation of albumin in a mouse model of nephrosis. Our data suggest that CUBAM and megalin albumin binding affinities are differentially tuned to mediate uptake of normally filtered versus pathological levels of albumin, respectively. Because KO of megalin in vivo ablates cubilin function in the kidney, it is not possible to determine whether CUBAM receptors can independently mediate uptake of normal albumin concentrations. However, a testable prediction of our hypothesis is that megalin (but not CUBAM) receptors can function independently to retrieve high concentrations of albumin filtered under nephrotic conditions. To test this hypothesis, we examined the requirement for

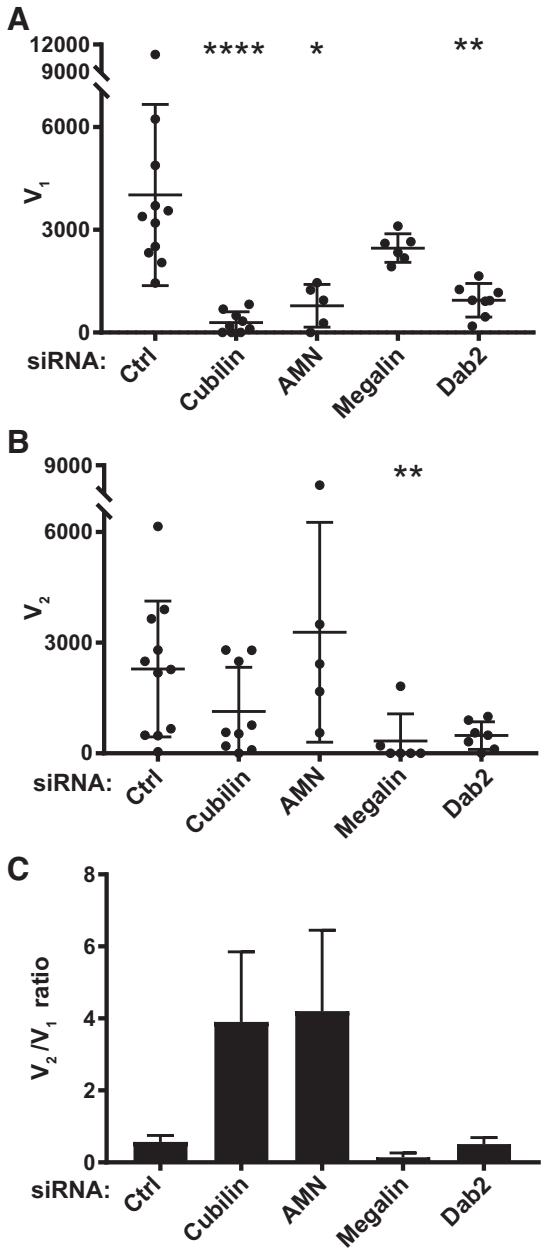

Fig. 4. Effect of cubilin, amnionless (AMN), megalin, and disabled-2 (Dab2) knockdown on high- and low-affinity albumin uptake capacity. The albumin uptake profile from each experiment was deconvolved, and high-affinity (V_1; *A*) and low-affinity (V_2; *B*) uptake capacities calculated for each condition are plotted as individual points with the mean and SD noted. Statistical significance was assessed by a Kruskal-Wallis test (one-way ANOVA with Dunn's multiple comparisons test. $*P \leq 0.01$, $**P < 0.05$, and $****P < 0.0001$ vs. control (Ctrl). *C*: ratio of V_2 to V_1 obtained from the mean V_2 and V_1 values from each group is plotted (means ± SE).

megalin and cubilin in PT albumin uptake in mouse kidney sections from inducible KO models variously targeting cubilin, megalin, and/or podocin (49, 50). Urinary albumin measurements in nephrotic megalin/cubilin KO mice confirmed a significant increase in albuminuria when the receptors are deleted; however, data for nephrotic mice with only megalin or cubilin KO are not available (49). In wild-type mice, low levels of albumin were clearly discernible within megalin- and cubilin-positive PT cells (Fig. 5*A*). No albumin was observed in PT cells in either megalin- or cubilin-KO mice (Fig. 5, *B* and *C*). As expected, PT cells in podocin KO mice accumulated much higher levels of albumin than wild-type mice (Fig. 5*D*) (49). Strikingly, albumin was efficiently internalized in PT cells of podocin/cubilin double-KO mice (Fig. 5*E*), suggesting that megalin receptor expression was sufficient to enable albumin retrieval of high [but not normal (Fig. 5*B*)] levels of albumin from the filtrate. Similarly, albumin uptake was only visible in PTs that expressed residual megalin after induction of podocin and megalin KO (Fig. 5*F*). Together, these data support the conclusion that CUBAM and megalin are both required for retrieval of normal levels of albumin, but that megalin can mediate cubilin-independent uptake of nephrotic levels of albumin.

Megalin-to-cubilin expression in OK cells and mouse kidneys. Albumin uptake measured in freshly isolated perfused rabbit PTs suggests that uptake capacity at high concentrations of albumin (≥2 mg/mL) is roughly 50-fold greater than at physiological concentrations (50 μg/mL) (37). In contrast, we measured only an approximately threefold increase in albumin uptake over this concentration range in our OK cells. It is possible that OK cells express less megalin and hence have fewer low-affinity albumin binding sites compared with PT cells in vivo. To test this possibility, we compared the relative expression of *LRP2* versus *CUBN* transcripts and megalin versus cubilin protein in the mouse kidney cortex versus OK cells. Because the primer efficiencies for each reaction may be different, we used ddPCR to obtain accurate values of mRNA transcript levels in each sample. As shown in Fig. 6, the ratio of *LRP2* to *CUBN* transcripts was 1.3-fold in OK cells and 3.5-fold in mice. This modest difference in ratios may reflect the preferential expression of megalin over cubilin in the PT S2 segment, where low levels of *CUBN* transcripts and cubilin protein levels have been reported (26, 43). Regardless, our data suggest that mouse kidney cortex and OK cells have comparable ratios of low-affinity to high-affinity albumin uptake sites and that differences in relative megalin expression likely do not account for the divergence in albumin uptake profiles between perfused PTs and OK cells.

Dab2, megalin, and cubilin knockdown inhibit fluid phase uptake in PT cells. At concentrations that saturate the low- and high-affinity uptake pathways, excess albumin will behave as a fluid phase marker. While PT cells do not apparently possess a clathrin-independent fluid phase uptake pathway, the robust endocytic activity in this nephron segment suggests that a substantial volume of PT filtrate is internalized within clathrin-coated vesicles (4). In vivo, loss of either Dab2 or megalin expression dramatically curtails formation of endocytic vesicles, suggesting that passive uptake of fluid phase markers will also be inhibited. Global fits of the data in Fig. 3 show that knockdown of megalin, cubilin, and especially Dab2 reduced the nonsaturable component of albumin uptake (C_3) compared with control. To examine fluid phase uptake independently, we compared the effects of receptor protein and Dab2 knockdown on the uptake of the fluid phase marker Alexa Fluor 647-dextran. Dextran uptake was roughly linear with increasing concentration as expected for uptake of a fluid phase marker (Fig. 7). Knockdown of Dab2 or megalin profoundly inhibited dextran uptake, whereas knockdown of cubilin had a more modest effect. Together, our data are consistent with a model

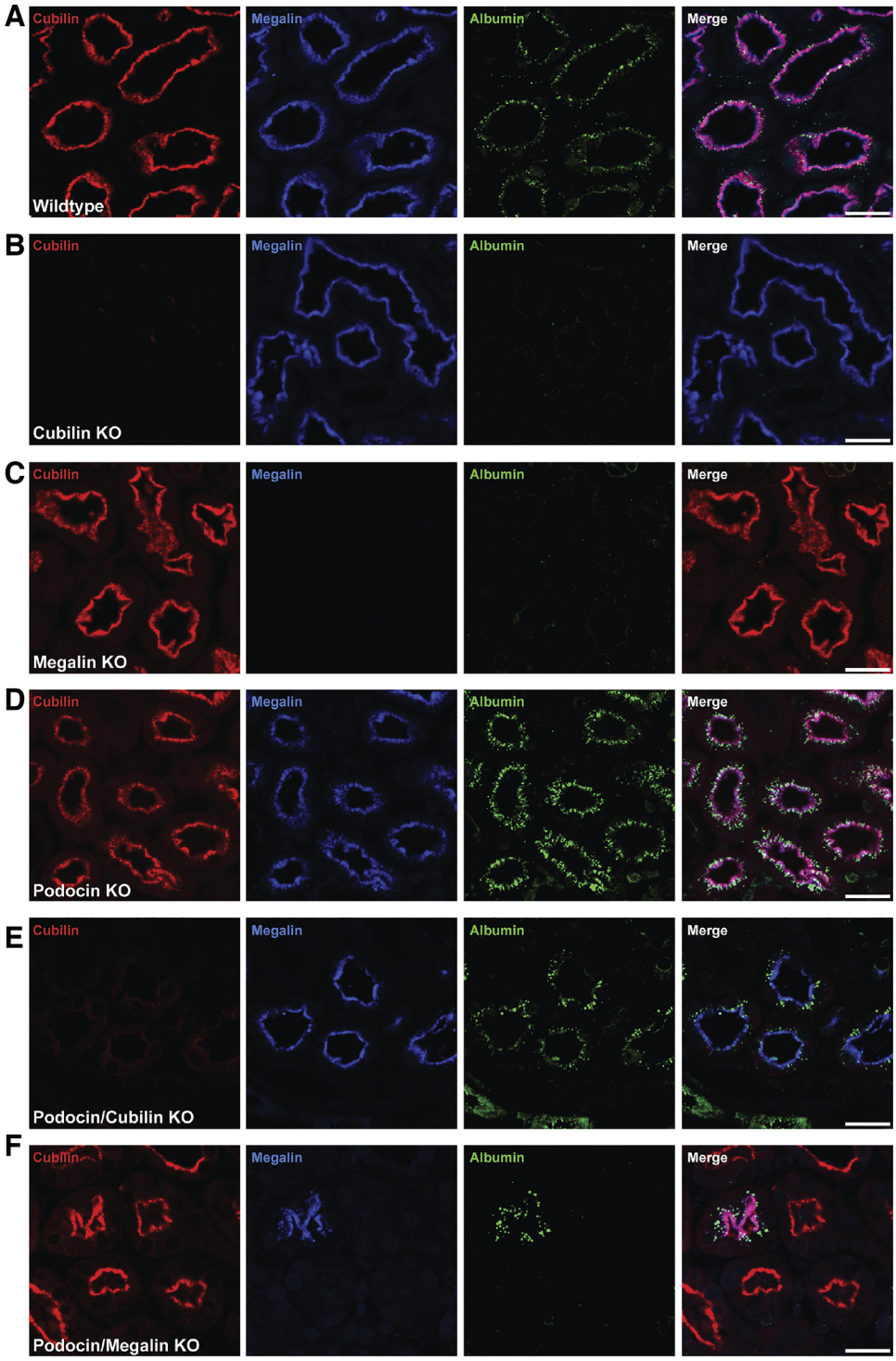

Fig. 5. Megalin takes up albumin independently of cubilin in nephrotic podocin knockout (KO) mice. *A*−*F*: immunostaining for cubilin (red), megalin (blue), and albumin (green) in kidney sections from control mice (*A*), inducible cubilin KO mice (*B*), inducible megalin KO mice (*C*), inducible podocin KO mice (*D*), inducible podocin/cubilin KO mice (*E*), and inducible podocin/megalin KO mice (*F*). Confocal images were taken at ×20 magnification. Scale bars = 40 μm. Only megalin- and cubilin-positive cells take up albumin in normal mice; under proteinuria, cubilin expression is dispensable for albumin uptake (but megalin is not).

in which passive uptake of albumin in the fluid phase contributes to retrieval of high concentrations of albumin.

DISCUSSION

The present study demonstrates that cubilin and megalin receptors are differentially involved in the reclamation of normal versus pathological levels of filtered albumin by PT cells. We observed a dose-dependent profile of albumin uptake consistent with the presence of a saturable low-affinity binding site in addition to the single high-affinity site for albumin binding observed in surface binding studies. The best global fit using data from multiple experiments also includes a component for nonsaturable uptake that likely reflects passive incorporation of fluid phase albumin into endocytic vesicles. Knockdown of cubilin or AMN selectively ablated uptake via the high-affinity site, confirming that recovery of normally filtered albumin is dependent on CUBAM receptor expression, as previously observed in mice (2, 50). In contrast, knockdown of

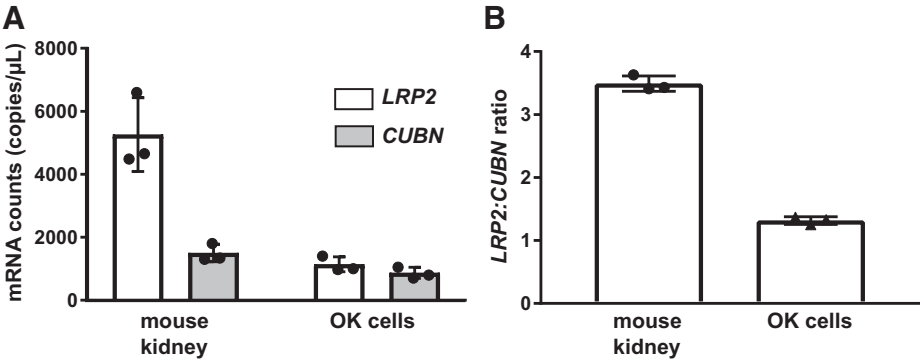

Fig. 6. Megalin [low-density lipoprotein-related protein 2 (*LRP2*)] to cubilin (*CUBN*) mRNA transcript ratios in opossum kidney (OK) cells and the mouse kidney. Digital droplet PCR was performed using validated primers for *LRP2* and *CUBN* to enable direct quantitation of mRNA transcript ratios in OK cells and in the mouse kidney cortex. Data from RNA isolated from 3 independent experiments are plotted. *A*: absolute mRNA transcript counts for *LRP2* and *CUBN* in the mouse kidney and OK cells are plotted. *B*: plot of the *LRP2*-to-*CUBN* transcript ratio in the mouse kidney and OK cells. The mean fold difference in *LRP2* over *CUBN* expression was 3.5 ± 0.12 and 1.3 ± 0.06 for the mouse kidney and OK cells, respectively.

megalin impaired the lower-affinity site for albumin uptake. Knockdown of Dab2 impaired uptake via both sites. Additionally, we observed effects on nonsaturable uptake. When we directly examined fluid phase uptake using labeled dextran, we found a dramatic reduction in cells depleted of Dab2 or megalin and a more modest effect of cubilin knockdown. Based on our results in cultured cells and studies in rodents, we propose a new model to explain how the PT accommodates efficient uptake across the wide range of tubular albumin concentrations in normal versus disease states.

Our conclusion that binding to cubilin is primarily responsible for the uptake of normally filtered albumin is bolstered by a recent study in humans demonstrating an association of albuminuria with mutations in *CUBN* (3). Patients with biallelic *CUBN* variants excreted roughly 20-fold more albumin than normal per day, consistent with observations in cubilin KO mice (50). This suggests that megalin in the PT has neither the affinity nor the capacity to reclaim significant levels of even normally filtered albumin, let alone nephrotic concentrations. Rather, these data support our model in which a primary function of megalin is to maintain cubilin-dependent uptake under normal conditions and to enable fluid phase uptake of albumin in nephrotic states. Additionally, megalin binds directly and with high affinity to many other filtered ligands and is required for their retrieval (6, 15, 16, 18–21, 23, 45).

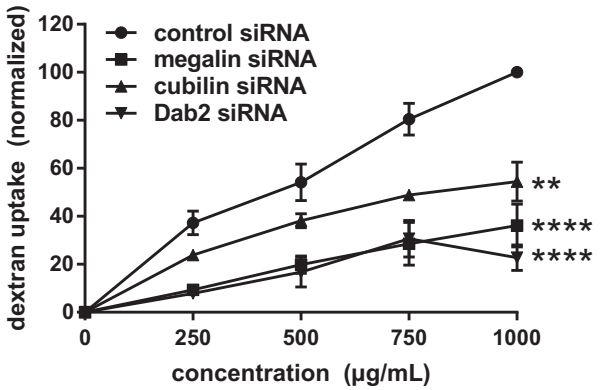

Fig. 7. siRNA knockdown of cubilin (*CUBN*), megalin [low-density lipoprotein-related protein 2 (*LRP2*)], or disabled-2 (Dab2) inhibits uptake of a fluid phase marker. Opossum kidney (OK) cells transfected with the indicated siRNAs were incubated with the 250–1000 µg/mL Alexa Fluor 647-dextran for 15 min at 37°C and then rapidly washed and solubilized, and cell-associated fluorescence was quantified. Mean uptake ± SD from 3 independent experiments are plotted, with maximal uptake in control cells normalized to 100%. Uptake at each time point for every condition was significantly different from control by two-way ANOVA (**$P > 0.002$; ****$P < 0.0001$).

We hypothesize that passive uptake of albumin via its fluid phase incorporation into endocytic vesicles contributes to the enormous reserve capacity for albumin uptake under nephrotic conditions. Uptake via this pathway in vivo is absolutely dependent on the expression of megalin, as we observed cubilin- but not megalin-independent accumulation of albumin in PTs of nephrotic mice. KO of megalin or Dab2 in mice has been previously observed to impair the elaboration of apical endocytic compartments (27, 33, 34). Consistent with this, we found that the nonsaturable component of albumin uptake and internalization of the fluid phase marker dextran were dramatically reduced in OK cells transfected with megalin or Dab2 siRNA. At first glance, it is surprising that megalin knockdown impaired fluid phase uptake without apparently impacting cubilin-mediated uptake of albumin. It is possible that CUBAM receptors are directed more efficiently into coated pits in the absence of megalin expression. Alternatively, megalin knockdown might impair endocytic pathway organization to redistribute more high-affinity (CUBAM) albumin binding sites to the plasma membrane. Finally, megalin expression may affect the size of endocytic vesicles, which would discoordinately affect uptake of membrane-bound versus fluid phase components.

An elegant recent study by Hall and colleagues (40, 43) demonstrated complete reabsorption of fluorescent albumin injected into the circulation by cells of the S1 segment of the PT. By contrast, uptake of fluid phase markers was low in the S1 segment but robust in S2 (43). Interestingly, whereas cubilin expression in S2 cells was highly variable, megalin was consistently expressed in the S2 segment. Connecting these results with our data here, we propose a novel model for the uptake of normal and nephrotic concentrations of albumin (Fig. 8). In our model, normally filtered albumin is retrieved exclusively in the S1 segment by CUBAM and/or megalin receptors. Under nephrotic conditions where receptor-dependent uptake pathways are saturated, water reabsorption via paracellular and transcellular transport will result in the delivery of progressively concentrated albumin into more distal segments of the proximal tubule. While some megalin-dependent uptake will occur via direct binding, we hypothesize that the primary role of megalin under these conditions is to maintain fluid phase uptake of increasingly concentrated albumin in the S2 and S3 segments. Preferential uptake of albumin in these later segments of the PT could account for the dramatic capacity

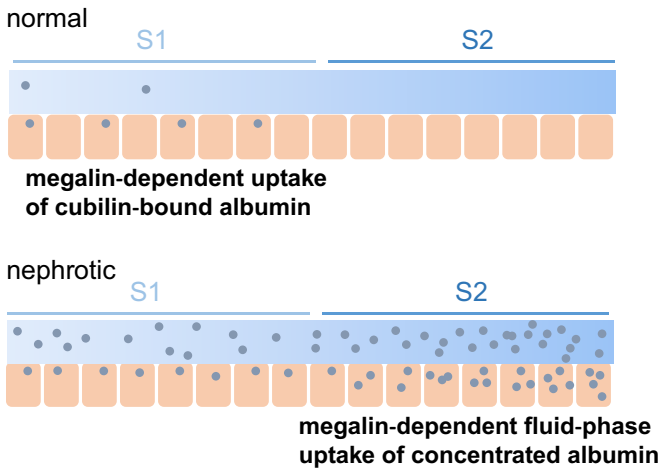

Fig. 8. Model for uptake of normal and nephrotic levels of albumin along the proximal tubule. Based on our data and published results by others, we hypothesize that normally filtered albumin is retrieved exclusively in the S1 segment by high-affinity binding to cubilin in association with amnionless (AMN) and/or megalin. Under nephrotic conditions where cubilin-mediated uptake is saturated, the concentration of albumin will increase progressively along the tubule as fluid is reabsorbed via paracellular and transcellular transport mechanisms. We hypothesize that passive uptake of albumin via its incorporation into endocytic vesicles whose formation requires the expression of megalin [and disabled-2 (Dab2)] accounts for the enormous reserve capacity for albumin uptake under nephrotic conditions. See the DISCUSSION for more details.

of the "low-affinity" uptake pathway previously described in perfused rabbit tubules in the landmark studies of Park and Maack (37).

The availability of our optimized OK cell culture model was instrumental in being able to segregate the contributions of megalin and cubilin to PT albumin uptake. OK cells cultured under our conditions have an approximately fivefold higher endocytic capacity compared with OK cells cultured under static conditions, which provided sufficient signal to deconvolve individual components from endocytic uptake curves. However, our data from OK cells also raise important questions that remain to be resolved. Our model is predicated on the assumption that the relative amounts (if not the absolute levels) of megalin and cubilin receptors in OK cells and the S1 segment of the PT are comparable. At present, we cannot quantitatively determine the levels of megalin and cubilin protein or their ratios in OK cells versus the mouse kidney. Even though antibodies exist that recognize similar regions of the proteins, the sequences in these regions differ between species and the affinities of these antibodies for mouse or opossum protein are likely different. An additional complication is that the expression of megalin and cubilin transcripts and proteins has been shown to vary along the length of the PT. That said, the approximately two- to fivefold difference in megalin and cubilin transcript abundance between mouse and opossum that we measured using ddPCR suggests that expression of these receptors is not hugely reduced in our cell culture model compared with PT cells in vivo.

An additional question raised by our study is why did knockdown of megalin in OK cells not impair high-affinity uptake of albumin, given that uptake of normally filtered albumin in vivo is clearly dependent on megalin expression? Although megalin knockdown was very efficient based on Western blot analysis and immunofluorescence, it is formally possible that a small amount of residual megalin is sufficient to maintain CUBAM function in OK cells. It is also possible, as noted above, that the endocytic pathway is impaired in megalin knockdown cells resulting in an increased number of high-affinity albumin surface binding sites. Alternatively, CUBAM receptors may function independently in OK cells, similar to their ability of CUBAM to internalize ligands in other cell types that do not express megalin (22, 38, 39). A recent high-resolution structure reveals a tight assembly of CUBAM consisting of three cubilin fragments bound to AMN, consistent with stable association of the complex after initial delivery to the cell surface (25). Additional studies are needed to illuminate how loss of megalin affects endocytic pathway organization and how interaction with megalin affects cubilin endocytosis. Current initiatives using CRISPR/Cas9 technology to knock out megalin and cubilin in OK cells will resolve this issue.

Our data have implications for the design of therapeutics to treat nephrotic syndrome proteinuria and also point to the need for further studies to clarify the role of fluid phase uptake in albumin uptake under nephrotic conditions. Uptake of excessive levels of filtered proteins in many nephrotic conditions is known to result in PT injury, mediated at least in part due to toxic molecules ferried by albumin (13). Increased uptake of fatty acid-bound albumin in S2 may also explain why this nephron segment is particularly sensitive to megalin-dependent toxicity in mice fed a high-fat diet (24). Our study suggests that cubilin expression is unlikely to contribute significantly to this cytotoxicity. Furthermore, our results suggest that maneuvers to limit water reabsorption or dampen Dab2 expression may be more beneficial in prolonging PT function during proteinuric assault compared with compounds that selectively target receptor-mediated uptake of albumin.

ACKNOWLEDGMENTS

We are grateful to the University of Pittsburgh Health Sciences Genomics Research Core for assistance with droplet digital PCR. We thank I. Blenker Kristoffersen, P. Kamuk Nielsen, H. Salling Gittens, and H. Sidelmann from the Department of Biomedicine, Aarhus University, for excellent technical assistance and G. Mollet and C. Antignac at INSERM for the podocin knockout mice.

GRANTS

This work was supported by National Institute of Diabetes and Digestive and Kidney Diseases (NIDDK) Grants R01-DK-101484, DK-100357, and DK-118726 (to O. A. Weisz) and DK-098204 (to O. B. Kashlan). Q. Ren was supported by the China Scholarship Council. K. Weyer, R. Nielsen, and E. I. Christensen were supported by the Danish Medical Research Council (K. Weyer: DFF 12-132499 and E. I. Christensen: DFF 4183-00014B) and the Aarhus University Research Foundation (K. Weyer: AUFF-E-2017-7-25). We are grateful to access to the cores of the Pittsburgh Center for Kidney Research funded by NIDDK Grant P30-DK-079307.

DISCLOSURES

No conflicts of interest, financial or otherwise, are declared by the author(s).

AUTHOR CONTRIBUTIONS

Q.R., K.W., O.B.K., and O.A.W. conceived and designed research; Q.R., K.W., Y.R., K.R.L., and C.J.B. performed experiments; Q.R., K.W., K.R.L., R.J.T., R.N., E.I.C., C.J.B., O.B.K., and O.A.W. analyzed data; Q.R., K.W., C.J.B., O.B.K., and O.A.W. interpreted results of experiments; Q.R., K.W., and O.A.W. prepared figures; O.B.K. and O.A.W. drafted manuscript; Q.R., K.W., Y.R., K.R.L., R.J.T., R.N., E.I.C., C.J.B., O.B.K., and O.A.W. edited

and revised manuscript; Q.R., K.W., Y.R., K.R.L., R.J.T., R.N., E.I.C., C.J.B., O.B.K., and O.A.W. approved final version of manuscript.

REFERENCES

1. **Ahuja R, Yammani R, Bauer JA, Kalra S, Seetharam S, Seetharam B.** Interactions of cubilin with megalin and the product of the amnionless gene (AMN): effect on its stability. *Biochem J* 410: 301–308, 2008. doi:10.1042/BJ20070919.
2. **Amsellem S, Gburek J, Hamard G, Nielsen R, Willnow TE, Devuyst O, Nexo E, Verroust PJ, Christensen EI, Kozyraki R.** Cubilin is essential for albumin reabsorption in the renal proximal tubule. *J Am Soc Nephrol* 21: 1859–1867, 2010. doi:10.1681/ASN.2010050492.
3. **Bedin M, Boyer O, Servais A, Li Y, Villoing-Gaudé L, Tête M-J, Cambier A, Hogan J, Baudouin V, Krid S, Bensman A, Lammens F, Louillet F, Ranchin B, Vigneau C, Bouteau I, Isnard-Bagnis C, Mache CJ, Schäfer T, Pape L, Gödel M, Huber TB, Benz M, Klaus G, Hansen M, Latta K, Gribouval O, Morinière V, Tournant C, Grohmann M, Kuhn E, Wagner T, Bole-Feysot C, Jabot-Hanin F, Nitschké P, Ahluwalia TS, Köttgen A, Andersen CBF, Bergmann C, Antignac C, Simons M.** Human C-terminal CUBN variants associate with chronic proteinuria and normal renal function. *J Clin Invest* 130: 335–344, 2019. doi:10.1172/JCI129937.
4. **Birn H, Christensen EI, Nielsen S.** Kinetics of endocytosis in renal proximal tubule studied with ruthenium red as membrane marker. *Am J Physiol Renal Physiol* 264: F239–F250, 1993. doi:10.1152/ajprenal.1993.264.2.F239.
5. **Birn H, Fyfe JC, Jacobsen C, Mounier F, Verroust PJ, Orskov H, Willnow TE, Moestrup SK, Christensen EI.** Cubilin is an albumin binding protein important for renal tubular albumin reabsorption. *J Clin Invest* 105: 1353–1361, 2000. doi:10.1172/JCI8862.
6. **Birn H, Zhai X, Holm J, Hansen SI, Jacobsen C, Christensen EI, Moestrup SK.** Megalin binds and mediates cellular internalization of folate binding protein. *FEBS J* 272: 4423–4430, 2005. doi:10.1111/j.1742-4658.2005.04857.x.
7. **Christensen EI, Birn H, Storm T, Weyer K, Nielsen R.** Endocytic receptors in the renal proximal tubule. *Physiology (Bethesda)* 27: 223–236, 2012. doi:10.1152/physiol.00022.2012.
8. **Christensen EI, Maunsbach AB.** Effects of dextran on lysosomal ultrastructure and protein digestion in renal proximal tubule. *Kidney Int* 16: 301–311, 1979. doi:10.1038/ki.1979.132.
9. **Christensen EI, Nielsen R, Birn H.** From bowel to kidneys: the role of cubilin in physiology and disease. *Nephrol Dial Transplant* 28: 274–281, 2013. doi:10.1093/ndt/gfs565.
10. **Coudroy G, Gburek J, Kozyraki R, Madsen M, Trugnan G, Moestrup SK, Verroust PJ, Maurice M.** Contribution of cubilin and amnionless to processing and membrane targeting of cubilin-amnionless complex. *J Am Soc Nephrol* 16: 2330–2337, 2005. doi:10.1681/ASN.2004110925.
11. **Cui S, Verroust PJ, Moestrup SK, Christensen EI.** Megalin/gp330 mediates uptake of albumin in renal proximal tubule. *Am J Physiol Renal Physiol* 271: F900–F907, 1996. doi:10.1152/ajprenal.1996.271.4.F900.
12. **Drake CJ, Fleming PA, Larue AC, Barth JL, Chintalapudi MR, Argraves WS.** Differential distribution of cubilin and megalin expression in the mouse embryo. *Anat Rec A Discov Mol Cell Evol Biol* 277A: 163–170, 2004. doi:10.1002/ar.a.10123.
13. **Erkan E.** Proteinuria and progression of glomerular diseases. *Pediatr Nephrol* 28: 1049–1058, 2013. doi:10.1007/s00467-012-2335-1.
14. **Eshbach ML, Sethi R, Avula R, Lamb J, Hollingshead DJ, Finegold DN, Locker JD, Chandran UR, Weisz OA.** The transcriptome of the *Didelphis virginiana* opossum kidney OK proximal tubule cell line. *Am J Physiol Renal Physiol* 313: F585–F595, 2017. doi:10.1152/ajprenal.00228.2017.
15. **Eshbach ML, Weisz OA.** Receptor-mediated endocytosis in the proximal tubule. *Annu Rev Physiol* 79: 425–448, 2017. doi:10.1146/annurev-physiol-022516-034234.
16. **Faber K, Hvidberg V, Moestrup SK, Dahlbäck B, Nielsen LB.** Megalin is a receptor for apolipoprotein M, and kidney-specific megalin-deficiency confers urinary excretion of apolipoprotein M. *Mol Endocrinol* 20: 212–218, 2006. doi:10.1210/me.2005-0209.
17. **Gekle M, Mildenberger S, Freudinger R, Silbernagl S.** Functional characterization of albumin binding to the apical membrane of OK cells. *Am J Physiol Renal Physiol* 271: F286–F291, 1996. doi:10.1152/ajprenal.1996.271.2.F286.
18. **Gonzalez-Villalobos R, Klassen RB, Allen PL, Johanson K, Baker CB, Kobori H, Navar LG, Hammond TG.** Megalin binds and internalizes angiotensin-(1-7). *Am J Physiol Renal Physiol* 290: F1270–F1275, 2006. doi:10.1152/ajprenal.00164.2005.
19. **Gonzalez-Villalobos R, Klassen RB, Allen PL, Navar LG, Hammond TG.** Megalin binds and internalizes angiotensin II. *Am J Physiol Renal Physiol* 288: F420–F427, 2005. doi:10.1152/ajprenal.00243.2004.
20. **Hvidberg V, Jacobsen C, Strong RK, Cowland JB, Moestrup SK, Borregaard N.** The endocytic receptor megalin binds the iron transporting neutrophil-gelatinase-associated lipocalin with high affinity and mediates its cellular uptake. *FEBS Lett* 579: 773–777, 2005. doi:10.1016/j.febslet.2004.12.031.
21. **Jensen D, Kierulf-Lassen C, Kristensen MLV, Nørregaard R, Weyer K, Nielsen R, Christensen EI, Birn H.** Megalin dependent urinary cystatin C excretion in ischemic kidney injury in rats. *PLoS One* 12: e0178796, 2017. doi:10.1371/journal.pone.0178796.
22. **Jensen LL, Andersen RK, Hager H, Madsen M.** Lack of megalin expression in adult human terminal ileum suggests megalin-independent cubilin/amnionless activity during vitamin B12 absorption. *Physiol Rep* 2: e12086, 2014. doi:10.14814/phy2.12086.
23. **Klassen RBS, Allen PL, Batuman V, Crenshaw K, Hammond TG.** Light chains are a ligand for megalin. *J Appl Physiol* 98: 257–263, 2005. doi:10.1152/japplphysiol.01090.2003.
24. **Kuwahara S, Hosojima M, Kaneko R, Aoki H, Nakano D, Sasagawa T, Kabasawa H, Kaseda R, Yasukawa R, Ishikawa T, Suzuki A, Sato H, Kageyama S, Tanaka T, Kitamura N, Narita I, Komatsu M, Nishiyama A, Saito A.** Megalin-mediated tubuloglomerular alterations in high-fat diet-induced kidney disease. *J Am Soc Nephrol* 27: 1996–2008, 2016. doi:10.1681/ASN.2015020190.
25. **Larsen C, Etzerodt A, Madsen M, Skjødt K, Moestrup SK, Andersen CBF.** Structural assembly of the megadalton-sized receptor for intestinal vitamin B_{12} uptake and kidney protein reabsorption. *Nat Commun* 9: 5204, 2018. doi:10.1038/s41467-018-07468-4.
26. **Lee JW, Chou C-L, Knepper MA.** Deep sequencing in microdissected renal tubules identifies nephron segment-specific transcriptomes. *J Am Soc Nephrol* 26: 2669–2677, 2015. doi:10.1681/ASN.2014111067.
27. **Leheste JR, Rolinski B, Vorum H, Hilpert J, Nykjaer A, Jacobsen C, Aucouturier P, Moskaug JO, Otto A, Christensen EI, Willnow TE.** Megalin knockout mice as an animal model of low molecular weight proteinuria. *Am J Pathol* 155: 1361–1370, 1999. doi:10.1016/S0002-9440(10)65238-8.
28. **Long KR, Shipman KE, Rbaibi Y, Menshikova EV, Ritov VB, Eshbach ML, Jiang Y, Jackson EK, Baty CJ, Weisz OA.** Proximal tubule apical endocytosis is modulated by fluid shear stress via an mTOR-dependent pathway. *Mol Biol Cell* 28: 2508–2517, 2017. doi:10.1091/mbc.e17-04-0211.
29. **Maack T, Johnson V, Kau ST, Figueiredo J, Sigulem D.** Renal filtration, transport, and metabolism of low-molecular-weight proteins: a review. *Kidney Int* 16: 251–270, 1979. doi:10.1038/ki.1979.128.
30. **Moestrup SK, Kozyraki R, Kristiansen M, Kaysen JH, Rasmussen HH, Brault D, Pontillon F, Goda FO, Christensen EI, Hammond TG, Verroust PJ.** The intrinsic factor-vitamin B12 receptor and target of teratogenic antibodies is a megalin-binding peripheral membrane protein with homology to developmental proteins. *J Biol Chem* 273: 5235–5242, 1998. doi:10.1074/jbc.273.9.5235.
31. **Moestrup SK, Nielsen S, Andreasen P, Jørgensen KE, Nykjaer A, Røigaard H, Gliemann J, Christensen EI.** Epithelial glycoprotein-330 mediates endocytosis of plasminogen activator-plasminogen activator inhibitor type-1 complexes. *J Biol Chem* 268: 16564–16570, 1993.
32. **Mollet G, Ratelade J, Boyer O, Muda AO, Morisset L, Lavin TA, Kitzis D, Dallman MJ, Bugeon L, Hubner N, Gubler M-C, Antignac C, Esquivel EL.** Podocin inactivation in mature kidneys causes focal segmental glomerulosclerosis and nephrotic syndrome. *J Am Soc Nephrol* 20: 2181–2189, 2009. doi:10.1681/ASN.2009040379.
33. **Morris SM, Tallquist MD, Rock CO, Cooper JA.** Dual roles for the Dab2 adaptor protein in embryonic development and kidney transport. *EMBO J* 21: 1555–1564, 2002. doi:10.1093/emboj/21.7.1555.
34. **Nagai J, Christensen EI, Morris SM, Willnow TE, Cooper JA, Nielsen R.** Mutually dependent localization of megalin and Dab2 in the renal proximal tubule. *Am J Physiol Renal Physiol* 289: F569–F576, 2005. doi:10.1152/ajprenal.00292.2004.
35. **Nielsen R, Mollet G, Esquivel EL, Weyer K, Nielsen PK, Antignac C, Christensen EI.** Increased lysosomal proteolysis counteracts protein accumulation in the proximal tubule during focal segmental glomerulosclerosis. *Kidney Int* 84: 902–910, 2013. doi:10.1038/ki.2013.218.

36. **Nykjaer A, Fyfe JC, Kozyraki R, Leheste JR, Jacobsen C, Nielsen MS, Verroust PJ, Aminoff M, de la Chapelle A, Moestrup SK, Ray R, Gliemann J, Willnow TE, Christensen EI.** Cubilin dysfunction causes abnormal metabolism of the steroid hormone 25(OH) vitamin D(3). *Proc Natl Acad Sci USA* 98: 13895–13900, 2001. doi:10.1073/pnas.241516998.
37. **Park CH, Maack T.** Albumin absorption and catabolism by isolated perfused proximal convoluted tubules of the rabbit. *J Clin Invest* 73: 767–777, 1984. doi:10.1172/JCI111270.
38. **Park J, Levic DS, Sumigray KD, Bagwell J, Eroglu O, Block CL, Eroglu C, Barry R, Lickwar CR, Rawls JF, Watts SA, Lechler T, Bagnat M.** Lysosome-rich enterocytes mediate protein absorption in the vertebrate gut. *Dev Cell* 51: 7–20.e6, 2019. doi:10.1016/j.devcel.2019.08.001.
39. **Pedersen GA, Chakraborty S, Steinhauser AL, Traub LM, Madsen M.** AMN directs endocytosis of the intrinsic factor-vitamin B_{12} receptor cubam by engaging ARH or Dab2. *Traffic* 11: 706–720, 2010. doi:10.1111/j.1600-0854.2010.01042.x.
40. **Polesel M, Hall AM.** Axial differences in endocytosis along the kidney proximal tubule. *Am J Physiol Renal Physiol* 317: F1526–F1530, 2019. doi:10.1152/ajprenal.00459.2019.
41. **Ren Q, Gliozzi ML, Rittenhouse NL, Edmunds LR, Rbaibi Y, Locker JD, Poholek AC, Jurczak MJ, Baty CJ, Weisz OA.** Shear stress and oxygen availability drive differential changes in opossum kidney proximal tubule cell metabolism and endocytosis. *Traffic* 20: 448–459, 2019. doi:10.1111/tra.12648.
42. **Sahali D, Mulliez N, Chatelet F, Laurent-Winter C, Citadelle D, Sabourin JC, Roux C, Ronco P, Verroust P.** Comparative immunochemistry and ontogeny of two closely related coated pit proteins. The 280-kd target of teratogenic antibodies and the 330-kd target of nephritogenic antibodies. *Am J Pathol* 142: 1654–1667, 1993.
43. **Schuh CD, Polesel M, Platonova E, Haenni D, Gassama A, Tokonami N, Ghazi S, Bugarski M, Devuyst O, Ziegler U, Hall AM.** Combined structural and functional imaging of the kidney reveals major axial differences in proximal tubule endocytosis. *J Am Soc Nephrol* 29: 2696–2712, 2018. doi:10.1681/ASN.2018050522.
44. **Schwegler JS, Heppelmann B, Mildenberger S, Silbernagl S.** Receptor-mediated endocytosis of albumin in cultured opossum kidney cells: a model for proximal tubular protein reabsorption. *Pflügers Arch* 418: 383–392, 1991. doi:10.1007/BF00550876.
45. **Seested T, Appa RS, Jacobsen C, Christensen EI.** Recombinant activated factor VII is reabsorbed in renal proximal tubules and is a ligand to megalin and cubilin. *Nephron Exp Nephrol* 117: e82–e92, 2011. doi:10.1159/000321161.
46. **Strope S, Rivi R, Metzger T, Manova K, Lacy E.** Mouse amnionless, which is required for primitive streak assembly, mediates cell-surface localization and endocytic function of cubilin on visceral endoderm and kidney proximal tubules. *Development* 131: 4787–4795, 2004. doi:10.1242/dev.01341.
47. **Tojo A, Endou H.** Intrarenal handling of proteins in rats using fractional micropuncture technique. *Am J Physiol Renal Physiol* 263: F601–F606, 1992. doi:10.1152/ajprenal.1992.263.4.F601.
48. **Wagner MC, Campos-Bilderback SB, Chowdhury M, Flores B, Lai X, Myslinski J, Pandit S, Sandoval RM, Wean SE, Wei Y, Satlin LM, Wiggins RC, Witzmann FA, Molitoris BA.** Proximal tubules have the capacity to regulate uptake of albumin. *J Am Soc Nephrol* 27: 482–494, 2016. doi:10.1681/ASN.2014111107.
49. **Weyer K, Andersen PK, Schmidt K, Mollet G, Antignac C, Birn H, Nielsen R, Christensen EI.** Abolishment of proximal tubule albumin endocytosis does not affect plasma albumin during nephrotic syndrome in mice. *Kidney Int* 93: 335–342, 2018. doi:10.1016/j.kint.2017.07.024.
50. **Weyer K, Storm T, Shan J, Vainio S, Kozyraki R, Verroust PJ, Christensen EI, Nielsen R.** Mouse model of proximal tubule endocytic dysfunction. *Nephrol Dial Transplant* 26: 3446–3451, 2011. doi:10.1093/ndt/gfr525.
51. **Zaias J, Mineau M, Cray C, Yoon D, Altman NH.** Reference values for serum proteins of common laboratory rodent strains. *J Am Assoc Lab Anim Sci* 48: 387–390, 2009.
52. **Zou Z, Chung B, Nguyen T, Mentone S, Thomson B, Biemesderfer D.** Linking receptor-mediated endocytosis and cell signaling: evidence for regulated intramembrane proteolysis of megalin in proximal tubule. *J Biol Chem* 279: 34302–34310, 2004. doi:10.1074/jbc.M405608200.

Supplementary Material Table of Contents

Table S1. siRNA sequences used in this study

ID	5'- sense sequence (+) -3'	3' overhang modification
siRNA2 *CUBN*	CCA ACG AAC UUG UGG AAA A	UU
siRNA2 *LRP2*	GGA AAG AGA UGC CGG CAA A	UU
siRNA3 *LRP2*	GGA GAG UGU UGA AGA UUU A	UU
siRNA9 *DAB2*	CCA CAU GAC UCC AUA ACA A	UU
siRNA4 *AMN*	CUG CCA ACU GGG ACA GAA A	UU
siRNA5 *AMN*	GGA CAG AAA CCG AAC UCC A	UU

Sequences used for RNAi experiments to knock down cubilin (*CUBN*), megalin (*LRP2*), Disabled-2 (*DAB2*), and amnionless (*AMN*). Similar results were obtained with all sequences listed for a given protein.

Table S2. qPCR primers used in this study

Gene name	PCR FORWARD PRIMER 5'_SEQ_3'	PCR REVERSE PRIMER 5'_SEQ_3'
ACTB	AGTACCCCATTGAACACGGT	GTCTCAAACATGATCTGTGTCATCT
CUBN	AAGAAGGAAAGGTCCTGCATGT	GTTCAGGAGGGTGACTAGAGC
AMN	ACCCTGTGGCAGAGATCAGA	GCATCTTCCACAACCACTTCT
LRP2	AGCCGGACCTGTGTTGATTT	AAATCAGAGATGCCACGCCA

Sequences used for qPCR experiments to quantify knockdown of cubilin (*CUBN*), megalin (*LRP2*), and amnionless (*AMN*) in OK cells. Data were normalized using the housekeeping gene *ACTB*.

Table S3. ddPCR primers and probes used in this study

ID	Primer 1: 5' to 3'	Primer 2: 5' to 3'	Probe: 5' to 3'	Target
CUBN_FAM	AGTATGAGGCAC AGAGTTTGG	ATGTGCTGGGTAG TTGTCAG	CGTCAATGTTGGAATCGT GGAGGTAGA	OK cells
LRP2_HEX	GTATCCCTCGAT CCTTTGTCTG	CATCACCATCACAA ACCCAAC	CCCAAGTGGCCGTTGCAT TCATC	OK cells

ID	Bio-Rad assay ID	Target
CUBN_FAM	dMmuCPE5114538	mouse
LRP2_HEX	dMmuCPE5121669	mouse

Sequences used for Droplet Digital PCR (ddPCR) experiments to quantify the ratio of megalin (*LRP2*): cubilin (*CUBN*) transcripts in mRNA isolated from OK cells and mouse kidney cortex.

Supplementary Figure Legends

Fig. S1. Validation of anti-cubilin antibody.
Polyclonal antibodies against the peptide sequence HDSNTDGYVTSPNYPDNYPAH within CUB domain 16 (amino acids 2229-2249) of *monodelphis domestica* that is 95% identical to *didelphis virginiana* and 80% identical to mouse (amino acids 2222-2244 of *mus musculus*) cubilin were raised in rabbits and affinity purified. (A) The antibodies recognize a primary band migrating well above 250 kDa, consistent with the predicted molecular mass of cubilin (460 kDa) in immunoprecipitates (lanes 2 and 3) or lysates of OK cells (lane 4) and mouse kidney cortex (lane 6) lysates after electrophoresis on Tris-Acetate gels. Lanes 1 and 5 contain molecular mass markers (migration marked in kDa on the left). (B) Indirect immunofluorescence of a mouse kidney section with anti-cubilin (red) and phalloidin (green) confirms apical and subapical staining consistent with the known localization of cubilin. Scale bar: 25 μm.

Fig. S2. Comparison of albumin uptake models.
Data were fit using a multi-component Hill-Langmuir equation (see eq. 1), with single values of K_i and H_i attributed to each pathway for all data sets, and individual values of V_i for each pathway for each data set. Model names, parameters (e.g. K_1, V_1, etc.), number of parameters, and goodness of fit ($\chi 2$) are shown for each model. Nested models (connected by dashed lines) were compared by F-test, with resulting p values shown. Fitting the data to a model with a single uptake pathway (Model A) resulted in fits with a clear pattern in the residual plot, suggesting a poor model. Adding a second pathway (Model C) reduced patterns in the residual plot and significantly improved the fit. In this model, K_2 fit to a value of 20300 ± 6900 μg/ml to account for nonsaturatable uptake we observed at high albumin concentrations, which we attributed to fluid-phase uptake. To determine whether these data were better described by 2 relatively high affinity uptake pathways, we fit our data to a 3 pathway model (Model E) while fixing K_3 to 20000 μg/ml to account for nonsaturatable uptake. Model E fit the data significantly better than the models with fewer components. We also considered cooperativity for each of the higher affinity components. While allowing cooperativity for the highest affinity pathway improved the single component model (Model B vs. A), it did not significantly improve fits for either the 2- or 3-component models (Model D vs. C, and Model F vs. H). Allowing cooperativity for the middle component in the 3-component model, did significantly improve the fit (Model G vs. E). However, a Hill coefficient of 1.26 ± 0.13 in Model G suggested little, if any cooperativity. We therefore selected Model E as the optimal model for our data.

Fig. S3. A non-saturable pathway contributes to uptake of high concentrations of albumin by OK cells.
OK cells were incubated with the indicated concentrations of AlexaFluor-647 albumin at 37ºC for 15 min in the absence (control, black) or presence of 100 mg/mL unlabeled albumin (duplicate samples, red), then rapidly washed, solubilized, and cell-associated fluorescent albumin assessed by spectrofluorimetry. Uptake curves were fitted as described in methods. The fit profiles are shown in black with raw data indicated by dots.

Fig. S4. Full length blots from Fig. 2A.
(A) Cells were transfected with the indicated siRNAs and cultured on Transwells as described in Methods. Samples were solubilized and equal protein loads were run on SDS-PAGE and western blotted to detect cubilin, megalin, or Dab2. Colorimetric and chemiluminescence images are merged to allow direct comparison of the blot profile with the molecular mass standards (in kDa) on the left.

Fig. S5. Amnionless knockdown phenocopies effect of cubilin siRNA.
(A) RNA samples from three independent siRNA experiments were analyzed by qPCR to quantify the effect of two different amnionless (*AMN*) siRNAs on expression of AMN, cubilin (*CUBN*), and megalin (*LRP2*) transcripts. Mean transcript levels (normalized to no siRNA control) +/- SD are plotted. *AMN* transcripts were reduced by 84% +/- 2.7 and 78% +/- 2.3 for *AMN* siRNA oligonucleotides 4 and 5, respectively, *p=0.0001 compared to cells transfected with control siRNA by one-way ANOVA with Dunnett's multiple comparisons test. *CUBN* and *LRP2* mRNA were unchanged from control. (B) Cells transfected with control siRNA or *AMN* siRNA were incubated with 40 μg/mL AlexaFluor 647-albumin,

then fixed and processed to detect actin and cubilin. AMN knockdown resulted in decreased cubilin staining and albumin uptake. Scale bar: 10 μm. (C) A representative albumin uptake curve (black) and deconvolution into high-affinity (C1, red), low-affinity (C2, green) and nonsaturable (C3, blue) components based on global fit are shown. The dotted line shows the control albumin uptake reproduced from Fig. 1B (note the different scale on the right y-axis) to highlight the effect of cubilin knockdown on uptake at low albumin concentrations.

Fig. S6. Raw data and residuals from global fitting.
Raw data from all profiles used to generate the best global fit is plotted on a linear (left) or semi-log (right) scale, with each curve representing a distinct kinetic profile. Residuals from each fit are color coded to match the curves and plotted above each dataset.

Fig. S7. Surface binding of albumin to OK cells reveals a single high-affinity site.
OK cells were incubated on ice for 30 min with the indicated concentration of AlexaFluor-647 albumin added apically, then washed rapidly five times and solubilized. Cell-associated albumin was quantified by spectrofluorimetry and plotted (circles). Nonspecific binding at each concentration was assessed in the presence of a 100-fold excess unlabeled albumin (squares). The K_m for albumin binding was 49 μg/mL. Similar results were obtained in three independent experiments. Note that the albumin binding capacity measured in surface assays is ≥50 fold lower than that taken up during a 15 min incubation at 37ºC.

Ren et al.
Fig. S1

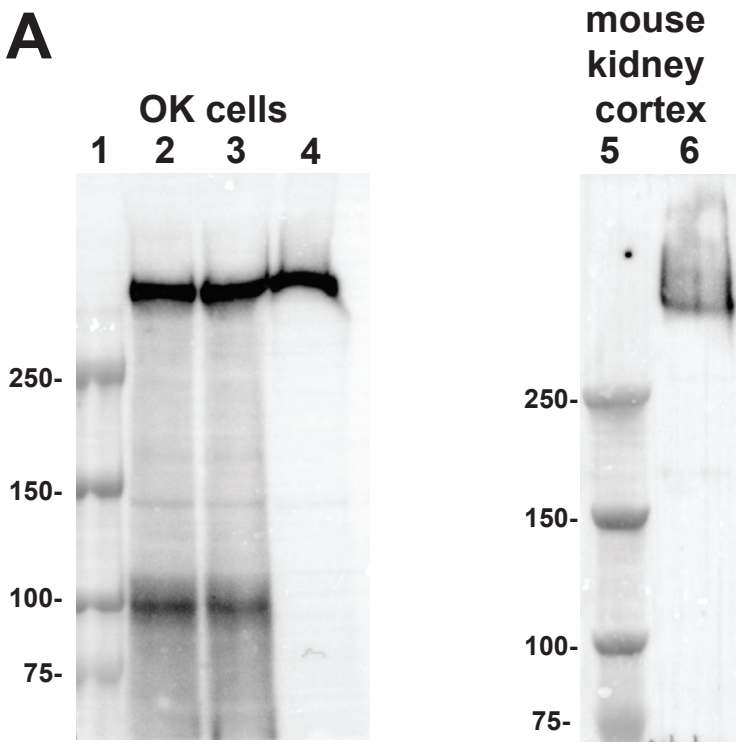

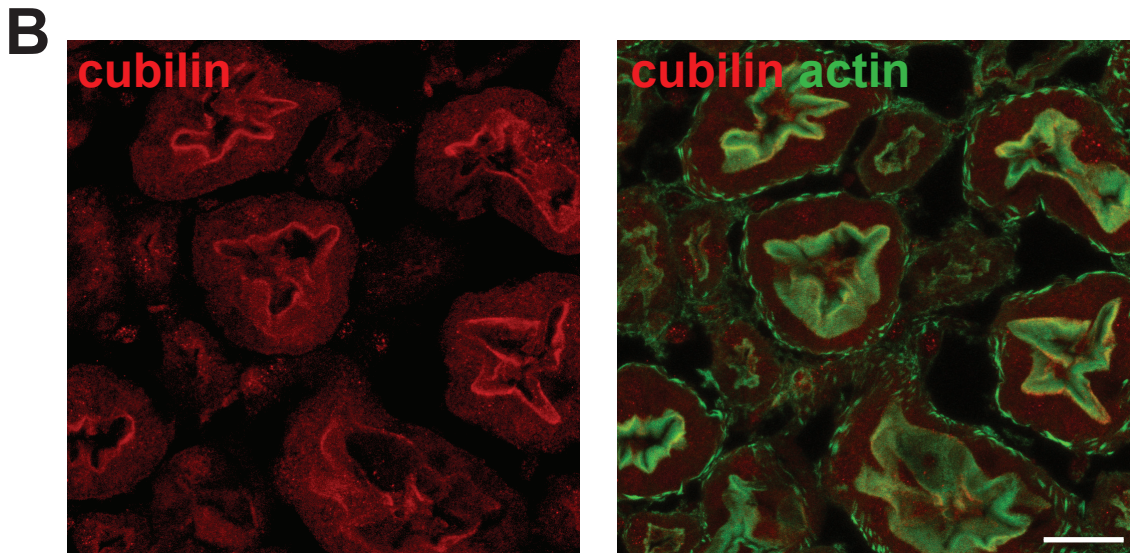

Ren et al.
Fig. S2

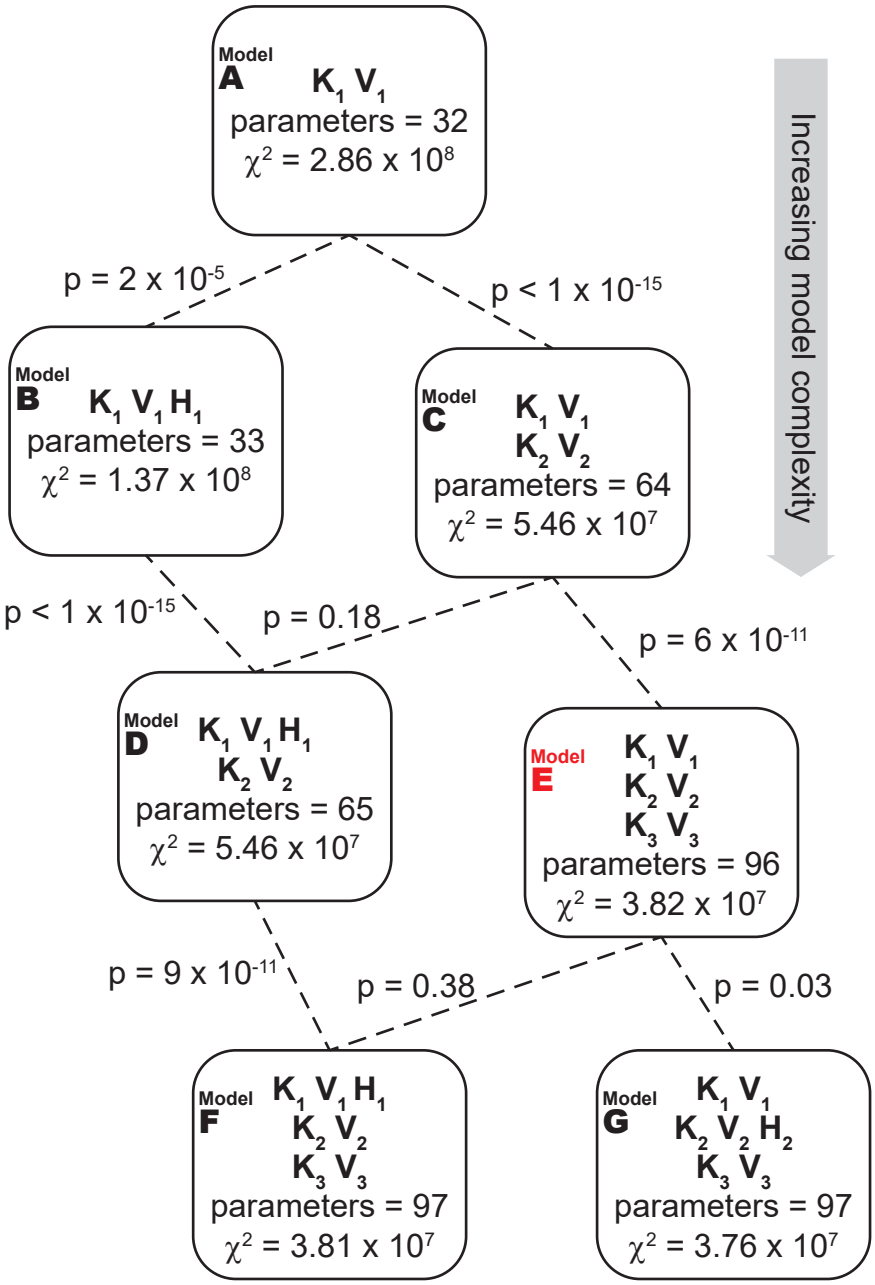

Ren et al.
Fig. S3

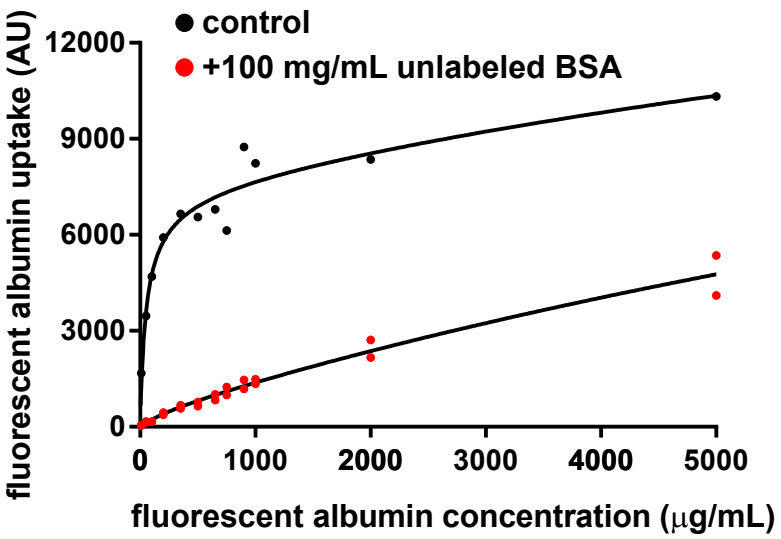

Ren et al.
Fig. S4

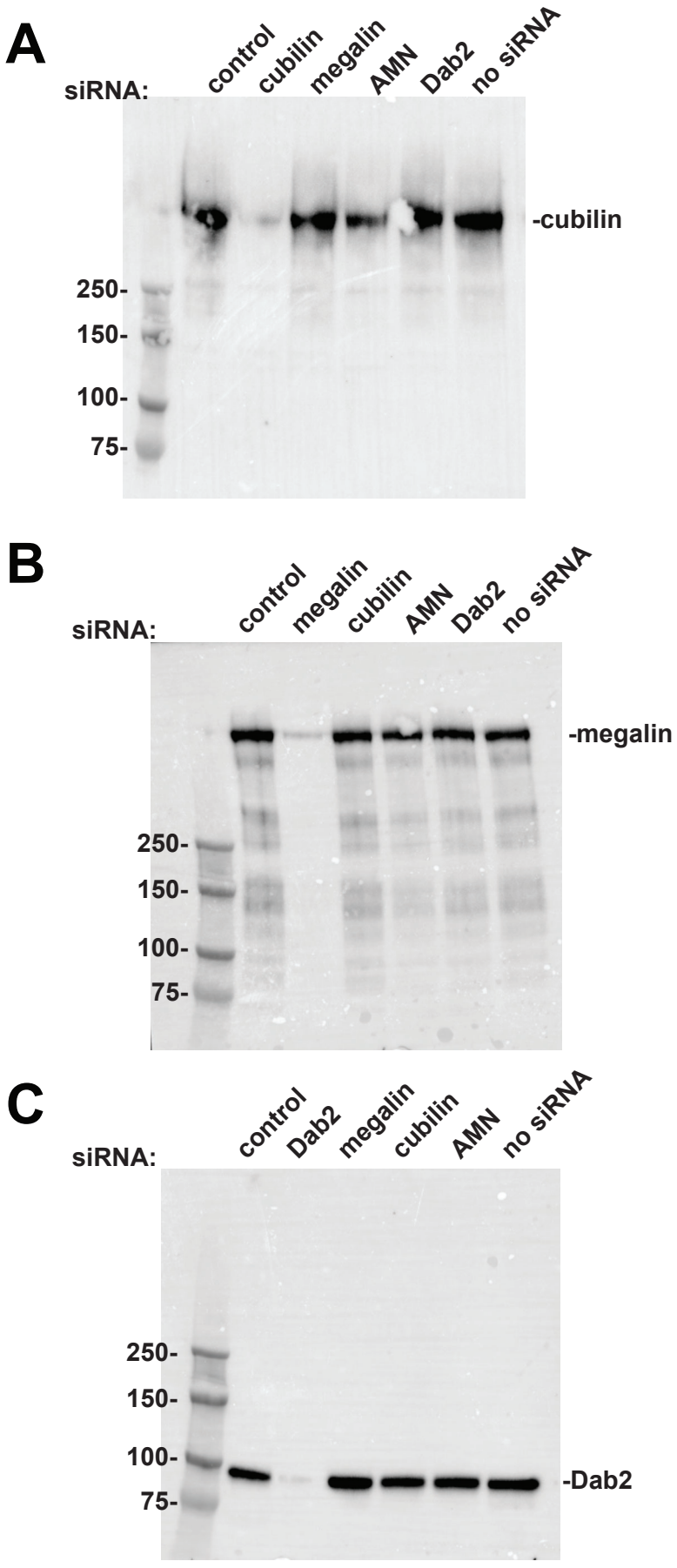

Ren et al.
Fig. S5

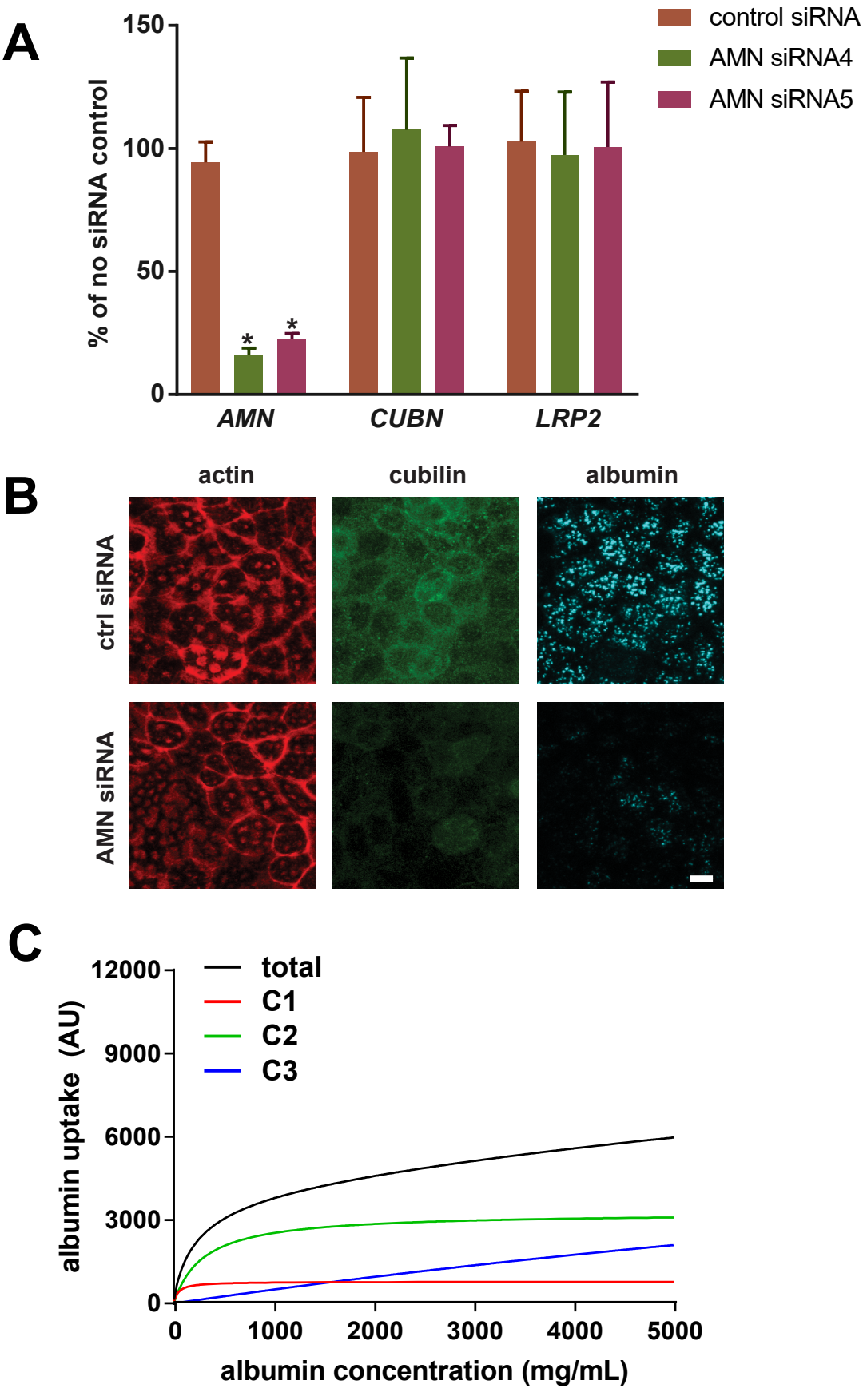

Ren et al.
Fig. S6

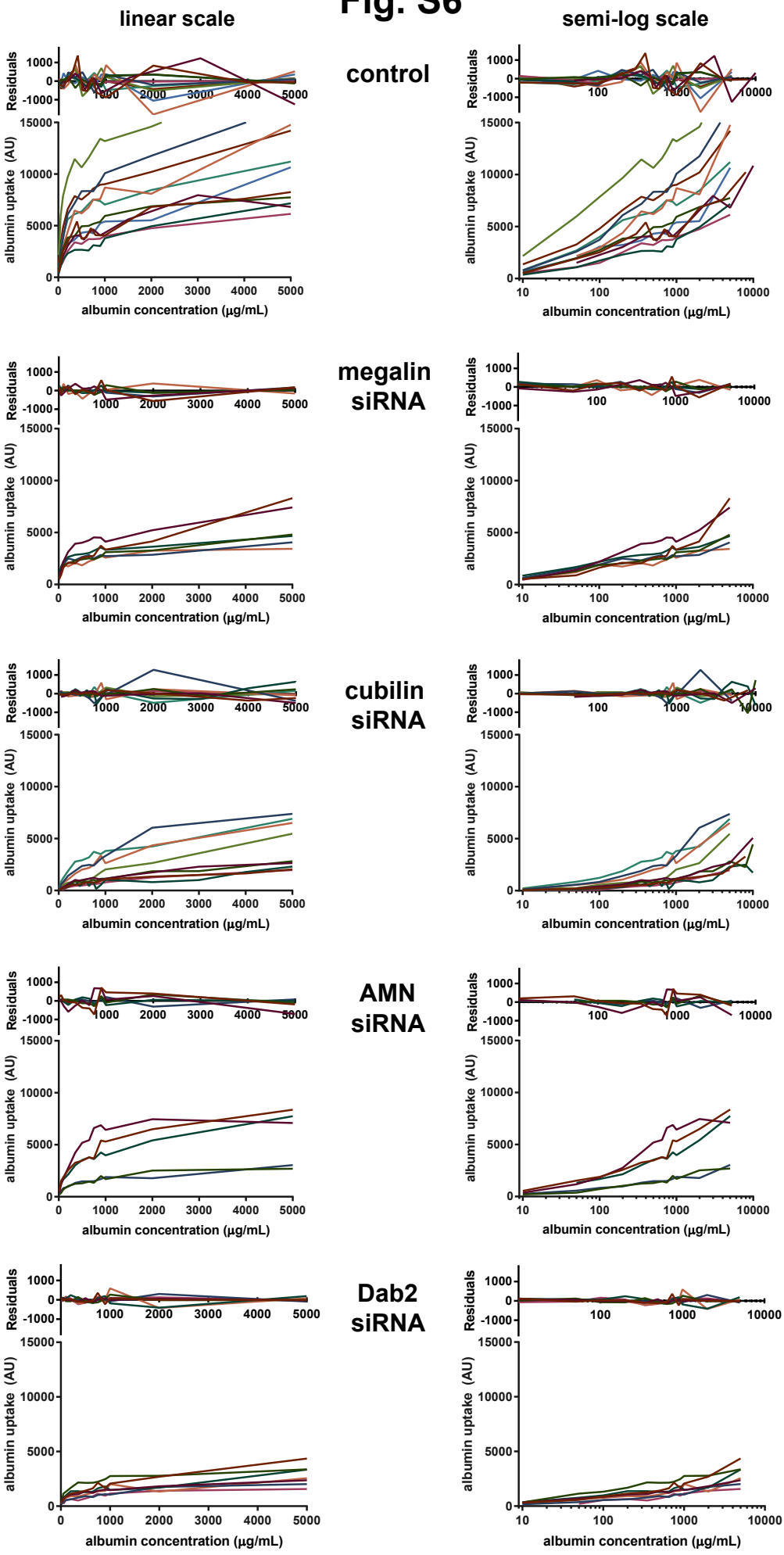

Ren et al.
Fig. S7